Structure-function coupling increases during interictal spikes in temporal lobe epilepsy: A graph signal processing study

I. Rigoni [a,*], J. Rué Queralt [b], K. Glomb [c], M.G. Preti [d,e,f], N. Roehri [a], S. Tourbier [b], L. Spinelli [a], M. Seeck [a], D. Van De Ville [d,e], P. Hagmann [b], S. Vulliémoz [a]

[a] EEG and Epilepsy Unit, University Hospital and Faculty of Medicine of Geneva, University of Geneva, Switzerland
[b] Department of Radiology, Lausanne University Hospital and University of Lausanne (CHUV-UNIL), Switzerland
[c] Brain Simulation Section, Berlin Institute of Health/Charite, 10098 Berlin, Germany
[d] Neuro-X Institute, School of Engineering, Ecole polytechnique fédérale de Lausanne, Geneva, Switzerland
[e] Department of Radiology and Medical Informatics, Faculty of Medicine, University of Geneva, Geneva, Switzerland
[f] CIBM Center for Biomedical Imaging, Switzerland

HIGHLIGHTS

- Structure-function coupling of interictal epileptic discharges (IEDs) was studied with graph signal processing for the first time.
- The predominance of smooth vs coarse spatial maps changes during the IED and points at stronger integration mechanisms during IEDs.
- This effect was localized in the ipsilateral mesial temporal regions of patients with temporal lobe epilepsy.

ARTICLE INFO

ABSTRACT

Objective: Structure-function coupling remains largely unknown in brain disorders. We studied this coupling during interictal epileptic discharges (IEDs), using graph signal processing in temporal lobe epilepsy (TLE).
Methods: We decomposed IEDs of 17 patients on spatial maps, i.e. network harmonics, extracted from a structural connectome. Harmonics were split in smooth maps (long-range interactions reflecting integration) and coarse maps (short-range interactions reflecting segregation) and were used to reconstruct the part of the signal coupled (Xc) and decoupled (Xd) from the structure, respectively. We analysed how Xc and Xd embed the IED energy over time, at global and regional level.
Results: For Xc, the energy was smaller than for Xd before the IED onset ($p < .001$), but became larger around the first IED peak ($p < .05$, cluster 2, C2). Locally, the ipsilateral mesial regions were significantly coupled to the structure over the whole epoch. The ipsilateral hippocampus increased its coupling during C2 ($p < .01$).
Conclusions: At whole-brain level, segregation gives way to integrative processes during the IED. Locally, brain regions commonly involved in the TLE epileptogenic network increase their reliance on long-range couplings during IED (C2).
Significance: In TLE, integration mechanisms prevail during the IED and are localized in the ipsilateral mesial temporal regions.

1. Introduction

Focal epilepsy is a disorder of brain networks (Laufs, 2012). Interictal epileptic discharges (IEDs) are used by clinicians on a daily basis to diagnose the disease and gain insight on the so-called epileptogenic network that is involved in the generation and propagation of epileptic seizures (Bartolomei et al., 2017). IEDs

have been the object of investigation of connectivity studies as they are the more evident epileptic signature on interictal electroencephalography (EEG) traces and are easier to capture than seizures. Past studies have suggested that higher levels of network integration during both IEDs and resting state are to be interpreted as markers of hyperexcitable pathologic activity, reflecting a greater extent of activity transfer within the epileptic network (Carboni et al., 2020, 2019). In support of such interpretation, higher interictal connectivity of regions not belonging to the epileptogenic zone as well as higher levels of global network integration during IEDs were associated with poor post-operative outcomes (Lagarde et al., 2018; Carboni et al., 2019).

Although it is still not understood how white matter connectivity gives rise to seizure dynamics, changes in structure–function (SF) coupling are known to occur in epilepsy. Studies using functional magnetic resonance imaging (fMRI) show that SF correlation is higher in right temporal lobe epilepsy (TLE) patients than in controls (Wirsich et al., 2016) but that it decreases in the limbic network of left TLE patients (Chiang et al., 2015) and in the language network during picture naming tasks (Trimmel et al., 2021). At the same time, intracranial EEG research reports that SF coupling increases from pre-ictal to ictal periods (Shah et al., 2019) and that it seems to predict post-surgery outcomes better than clinical parameters (Sinha et al., 2022). These heterogeneous findings illustrate the need for further investigation of SF coupling during interictal activity in TLE patients.

Graph signal processing (GSP) allows us to investigate brain connectivity patterns by including information about the structural connections that constrain the functional connectivity (Sorrentino et al., 2021). In practical terms, GSP is a framework that reinterprets common signal processing operations in a graph context (Shuman et al., 2013). Here, the signal to be processed is the functional brain signal –IEDs measured by EEG- and the graph on which the operations are performed is the structural connectome (SC). Using GSP, building blocks of the brain signal on the graph can be obtained via the so-called graph Laplacian, which is derived directly from the SC. In particular, "network harmonics" (NHs) (Glomb et al., 2020; Rué-Queralt et al., 2021) are the eigenvectors of the SC Laplacian, ordered according to increasing eigenvalue, which plays the role of graph frequency that reflects the increasing amount of variations along the brain graph (Atasoy et al., 2016; Ortega et al., 2018). The first low frequency (LF) harmonics, on the one hand, represent smooth gradients without much variation, capturing the main geometry of brain graph organization and long-range connections. The higher frequency (HF) harmonics, on the other hand, capture more localized patterns, less constrained by the white matter connectivity, and encapsulate short-range connections between neighboring brain regions. As in the time-domain, we can filter the functional signal by rewriting it as a linear combination of a subset of these spectral components (Shuman et al., 2013). If the LF harmonics are used, we reconstruct the part of the signal that is more "coupled" to structural connections; if the HF harmonics are used instead, we reconstruct the signal that moves more freely on the SC and that can be therefore considered more "decoupled" from the structure (Preti and Van De Ville, 2019). The structural-decoupling index (SDI) reflects the ratio between the energy of the decoupled and coupled signals in each brain region, allowing to quantify the regional level of SF coupling (Preti and Van De Ville, 2019).

This GSP-pipeline, applied on both resting state and task-related fMRI data, showed that low-level processing areas such as visual, auditory and somatomotor regions are more coupled to the SC, while high-level processing regions are less constrained by the structural connections (Preti and Van De Ville, 2019). Moreover, this SF coupling performed very accurately for task decoding and individual fingerprinting and, in particular, the more liberal

part of the signal appeared to yield key information for fingerprinting (Griffa et al., 2022). GSP was also applied to EEG data recorded during a face detection task (Glomb et al., 2020; Rué-Queralt et al., 2021). An alternation between time windows with signal energy concentrated in the LF harmonics –signaling long-range integrative patterns- and windows where HF harmonics prevailed -signaling focal, short-range segregation mechanisms- was interpreted as a succession of processing stages (Rué-Queralt et al., 2021).

Here, we used a pipeline previously tested on healthy subjects during evoked potentials (Glomb et al., 2020; Rué-Queralt et al., 2021) to distinguish between integration and segregation mechanisms during IEDs by projecting the EEG signal respectively on the LF and HF harmonics and studying their energy distribution in time and in space. We hypothesized that an increase of global network integration would be observed around the peak of the spike, reflecting the propagation process of the IED to the rest of the irritative network. We also investigated the regional SF coupling using the SDI.

2. Methods

2.1. Participants

In this retrospective study, 17 patients (median age 33 yrs, range 15–56 yrs, 5 females) diagnosed with TLE were selected from the research database of high-density EEG (HD-EEG) recorded at the epilepsy unit of the University Hospital of Geneva. Eight patients with left TLE (LTLE) and nine patients with right TLE (RTLE) were selected (see Table 1 for patients' details) based on the following inclusion criteria: diagnosed with TLE, available HD-EEG with IEDs and available structural MRI. At our centre, HD-EEG is routinely performed for the presurgical work-up and the reuse of this clinical data has been approved by the local ethics committee (CER 2020-02526).

2.2. Data acquisition and preprocessing

2.2.1. EEG

In the context of pre-surgical evaluation, a HD-EEG (129 or 257 channels, Electrical Geodesic Inc. system, sampling rate = 1000 Hz) is recorded overnight. From the recordings available, IEDs were identified and revised by a board-certified EEG expert (SV) and extracted for further analyses. IEDs that occurred less than 1 second apart were discarded. Epochs of 4 seconds, centered at the IED peak with highest amplitude, were extracted for each patient, preprocessed and used to reconstruct the electrical activity in $N = 118$ regions of interest (ROI). Epochs containing motion artifacts or eye-blinks were discarded after visual inspection. Selected data were band-pass filtered between 1 and 40 Hz, notch-filtered at 50 Hz and downsampled to 250 Hz. Channels with poor signal to noise ratio were identified as those with a standard deviation -computed across epochs- exceeding the third quartile by a factor of 1.5 times the interquartile range: these were replaced by a 'spline' interpolation of the neighboring channels (Perrin et al., 1989). Finally, the epochs were referenced to the average, further cropped to epochs of 1 second ($[-0.5 \ 0.5]$) and source-reconstructed (see Fig. 1).

2.2.2. MRI

T1 weighted MRI: An individual structural MRI image, namely a T1 weighted magnetization-prepared rapid acquisition gradient echo (MPRAGE), recorded in a 3 T scanner (Siemens Prisma), was available for each patient as part of the state-of-the-art clinical epilepsy MR imaging. The scans were resampled to 1 mm^3 isotropic resolution using cubic interpolation and the gray matter was par-

Table 1

Patients' characteristics, including the number of IEDs analyzed after removing those containing artefacts. F = female; M = male; R = right; L = left; ILAE = International League Against Epilepsy; IED = interictal epileptic discharge.

| Pat ID	Sex	Age when epilepsy started (years)	Age of recording (years)	Duration of disease (years)	Handedness	Etiology (MRI and histology)	Localisation	ILAE-class outcome	Follow -up (months)	Number of IEDs analyzed
P1	F	25	30	5	R	Mesial temporal dysplasia	Temporal R	5	21	40
P2	M	22	28	6	R	Hippocampal sclerosis	Temporal L	1	12	20
P3	M	27	51	24	R	Hippocampal sclerosis	Temporal L	1	12	55
P4	M	25	31	6	R	Hippocampal sclerosis	Temporal R	1	36	16
P5	M	1	15	14	R	Mesial temporal dysplasia	Temporal L	1	15	33
P6	M	17	44	27	R	Hippocampal sclerosis	Temporal L	1	60	12
P7	F	26	29	3	R	Mesial temporal glioma	Temporal L	1	12	9
P8	M	5	53	48	R	Hippocampal sclerosis	Temporal L	1	12	11
P9	M	11	16	5	R	Hippocampal sclerosis	Temporal R	1	36	26
P10	M	5	27	22	R	Hippocampal sclerosis	Temporal R	1	12	28
P11	M	15	33	18		Not lesional	Temporal L	3	3	14
P12	F	25	56	31	R	Hippocampal sclerosis	Temporal R	1	12	25
P13	M	23	27	4	R	Hippocampal sclerosis	Temporal R	1	36	29
P14	F	12	50	38	R	Hippocampal sclerosis	Temporal R	1	60	8
P15	F	16	51	35	L	Hippocampal sclerosis	Temporal L	1	24	33
P16	M	19	36	17	R	Not lesional	Temporal R	4	18	19
P17	M	19	34	15	R	Hippocampal sclerosis	Temporal R	1	9	21
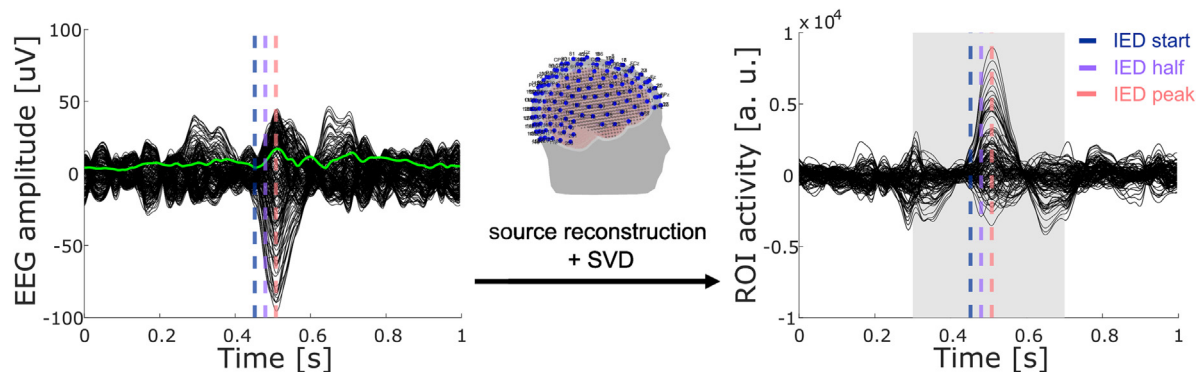
Fig. 1. The source reconstruction of the average interictal epileptic discharge (IED) of a patient. On the left, the spike, averaged across trials and displayed for the 204 channels. On the right, the same EEG time-course reconstructed in the brain region space, displayed for 118 regions of interest (ROI). In the middle, the patient-specific headmodel. The dashed vertical lines depict the start, half-rise and peak of the IED, calculated across patients.

celed in 128 ROI based on the second scale of Lausanne 2008 parcellation (Cammoun et al., 2012; Hagmann et al., 2008), using Freesurfer v6.0.1 and the Connectome Mapper (v3.0.0-beta-RC1) open-source pre-processing software (Tourbier et al., 2022, 2020). Ten subcortical structures (thalamus, caudate, putamen, pallidum and accumbens area) were removed and a total of $N = 118$ ROIs were retained for source reconstruction.

Diffusion weighted MRI: As standardized diffusion MRI is not part of the routine pre-clinical evaluation, we used an online available dataset consisting of 70 healthy participants to create a generic structural connectivity matrix (Griffa et al., 2019). The subjects were scanned in a 3 T scanner (Trio, Siemens Medical, Germany) with a 32-channel head-coil. As previously described, the subjects of the dataset were scanned with a diffusion spectrum imaging (DSI) sequence (Rué-Queralt et al., 2021) and MPRAGE, and tractography was performed on the DSI data following the protocol described in (Wedeen et al., 2008). In detail, the grey matter was segmented from the MPRAGE scans of the healthy subjects and parceled into 128 ROI according to the scale 2 of the Lausanne 2008 atlas. The reconstructed DSI data were used to estimate 70 structural connectivity matrices by deterministic streamline tractography. The number of fibers found between each voxel at the gray/white matter interface was summed within each brain area. A consensus connectome W was then obtained as previously

reported (Rué-Queralt et al., 2021) – with $N = 118$ ROI retained (same as above)- and was used for the extraction of the network harmonics (see Section 2.4).

2.3. Functional data – EEG source reconstruction

The EEG forward model was computed with the boundary element method for a three-layer model using OpenMEEG (Gramfort et al., 2011), starting from the individual resampled MRI scan. Solution points were imposed on a 5 mm grid located in the patient's gray matter and were unconstrained, meaning that each dipole had a three-dimensional orientation. The 129- and 257- electrodes EEG caps were manually coregistered to a template MRI scan and automatically warped to the individual MRI scan. Electrodes on the cheeks and neck were removed, leaving 109 and 204 channels, respectively, for the forward and inverse solution (Vorderwülbecke et al., 2020). For the latter, the electrical activity was reconstructed at the source level with exact low-resolution brain electromagnetic tomography (eLORETA) (Pascual-Marqui, 2007), with a regularization parameter value set to 0.05.

The three-dimensional information available at each solution point was summarized within each ROI ($N = 118$) as the first left singular vector, weighted by its singular value, resulting from a single value decomposition (SVD) performed across the concate-

nated epochs (Rubega et al., 2019). The ROI for which the neural time-courses were reconstructed were the same ROI that constituted the nodes of the consensus connectome W.

EEG preprocessing and source reconstruction were implemented in Matlab, using the Fieldtrip Toolbox (Oostenveld et al., 2011).

2.4. Structural data – Network harmonics

The network harmonics are defined as the eigenvectors of the graph Laplacian of the consensus structural connectome W. First, the symmetrically normalized graph Laplacian L of W is calculated as:

$$L = 1 - D^{-\frac{1}{2}} * W * D^{-\frac{1}{2}}$$

where D is the degree matrix of W, which is the diagonal matrix with the number of connections of each node. Then the eigenvectors U and eigenvalues Λ of L are extracted from the eigendecomposition $L = U\Lambda U^T$. The columns of U, $u_1 \ldots u_N$, are the eigenvectors of the graph Laplacian, the so-called network harmonics. These are associated with the corresponding eigenvalues $\lambda_1 \ldots \lambda_N$, which have increasing values and are ordered according to the smoothness of the network harmonics (eigenvectors) on the graph W. The smoothness of the eigenvector u_i measures the differences between connected nodes and therefore reflects the amount of variation along the gradient. U_i is smooth if neighboring nodes have similar values. Eigenvectors with increasing eigenvalues have decreasing smoothness, meaning that the variations along the cortex become less gradual and more abrupt (see Fig. 2). Each network harmonic is N-dimensional and identifies a specific brain pattern or spatial map. Refer to (Ortega et al., 2018; Shuman et al., 2013) for more details.

2.5. Graph signal processing

2.5.1. Graph Fourier transform

The graph Fourier transform (GFT) is the operation through which the EEG time-courses – reconstructed in the ROI-space – are mapped onto the space defined by the $u_1 \ldots u_N$ harmonics. Here, the ROI time-series data of each subject is an array of dimensions N × T × E, where N is the number of ROI ($N = 118$), T is the number of time points ($T = 100$, for 400 ms sampled at 250 Hz) and E is the number of epochs that varies across patients. Each N × 1 × 1 column of this 3-dimensional array, $x_e(t)$, is the source-reconstructed electrical activity of each ROI at the specific time point t of the epoch e. Being U the N × N matrix where each column is a NH, the GFT of $x_e(t)$ is defined as follows (Shuman et al., 2013):

$$\widehat{x}_e(t) = GFT\{x_e(t)\} = U^T * x_e(t).$$

As the graph spectral coefficients $\widehat{x}_e(t)$ describe the participation of each network harmonic to the original signal $x_e(t)$ at each time point, we refer to it as the "connectome spectrum" of the original ROI-based signal.

The original ROI-traces can then be retrieved via the inverse GFT (iGFT):

$$x_e(t) = iGFT\{\widehat{x}_e(t)\} = U * \widehat{x}_e(t)$$

2.5.2. Spectrum dichotomization

For each patient and epoch, the ROI time-courses were further cropped to epochs of 400 ms ([−0.2 0.2]), z-scored along time and graph Fourier transformed.

The graph power spectral density (gPSD) of $x_e(t)$ was calculated as the squared-value of the graph Fourier transform ($|\widehat{x}_e(t)|^2$), averaged over time and further averaged over epochs. We defined then a cut-off frequency λ_C as the frequency that divided the gPSD in two parts of equal cumulative power, i.e. area-under-the-curve (Preti and Van De Ville, 2019). Differently from what was previously proposed, the patients' individual variability was taken into account by selecting a cut-off frequency for each patient, rather than selecting a cut-off frequency based on a group-average gPSD (see Fig. 2). In other words, we calculated the patient-specific gPSD and λ_C.

We then used the first lowest C and the last highest $N - C$ harmonics to reconstruct the original ROI time-courses, resulting in

$$x_{C,e}(t) = U^{(low)} * \widehat{x}_e(t)$$
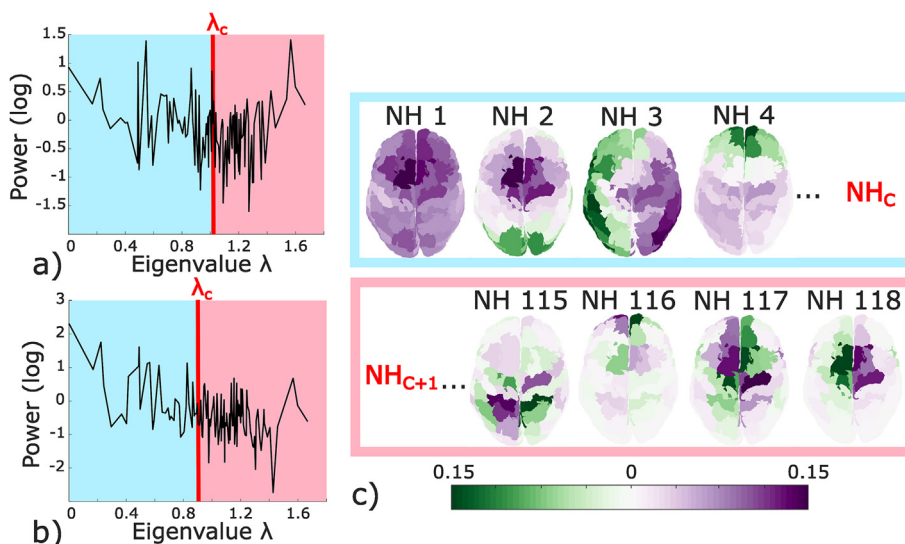
$$x_{D,e}(t) = U^{(high)} * \widehat{x}_e(t)$$

Fig. 2. Graph power spectral density of one RTLE patient (a) and one LTLE patient (b) and the network harmonics (NH). The vertical red line indicates the cut-off frequency λ_C defined for each patient, individually. In the first case, $\lambda_C = 52$; in the second, $\lambda_C = 38$. λ_C separates the low frequency harmonics (in light blue) from the high frequency ones (light red). On the right, the first four LF harmonics and the last four HF ones are depicted (c). The LF harmonics (NH_1, NH_2, ..., NH_C) are used to reconstruct the "coupled" part of the ROI time-courses; the HF harmonics (NH_{C+1}, NH_{C+2}, ..., NH_{118}) are used to reconstruct the "decoupled" part.

where $U^{(low)}$ and $U^{(high)}$ are the $N \times N$ matrices containing only the first C low-frequency harmonics and the last $N - C$ harmonics respectively, complemented with zeros, $x_{C,e}(t)$ is the filtered signal (in ROI-space) mostly coupled to the underlying structure and $x_{D,e}(t)$ the decoupled one.

To follow the dynamics of the energy distribution in the upper and lower end of the spectrum, the coupled and decoupled time-series were summarized over the space dimension (ROI) into two normalized energy time-courses:

$$E_{L,e}(t) = \frac{\|x_{C,e}(t)\|_2}{\|x_e(t)\|_2}$$

$$E_{H,e}(t) = \frac{\|x_{D,e}(t)\|_2}{\|x_e(t)\|_2}$$

where the numerator is the l_2-norm of the filtered signal taken, for each time point and epoch, over the ROI dimension, divided by the same l_2-norm of the original (unfiltered) ROI time-course. As computing the l_2-norm of a signal corresponds to compute the squared value of its energy calculated in the spatial domain (over ROI), $E_{L,e}(t)$ and $E_{H,e}(t)$ reflect, at each time point, the normalized amount of energy of the original ROI time-course $x_e(t)$ contained in the lowest- and highest-end of the spectrum (Rué-Queralt et al., 2021). $E_{L,e}(t)$ and $E_{H,e}(t)$ were then averaged across the epochs available for each patient and retained for compactness and broadcasting analyses. We will refer to these values as to $E_L(t)$ and $E_H(t)$.

2.6. Graph signal processing analyses

2.6.1. Whole-brain integration and segregation along the IED

Given that functional integration is the ability to rapidly combine specialized information from distributed brain regions (Rubinov and Sporns, 2010) and that LF harmonics capture smooth, long-range couplings, we interpret $E_L(t)$ as representative of integrative processes (Rué-Queralt et al., 2021; Wang et al., 2019). Contrarily, considering that functional segregation is the ability for specialized processing to occur within densely interconnected groups of brain regions (Rubinov and Sporns, 2010) and that HF harmonics capture focal, short-range couplings, we interpret $E_H(t)$ as representative of segregative processes (Rué-Queralt et al., 2021; Wang et al., 2019).

To detect whether integration and segregation mechanisms prevailed at any point in time during the IED, we used a cluster-based permutation test on the $E_L(t)$ and $E_H(t)$ time courses (Maris and Oostenveld, 2007). The null distribution was generated by randomly swapping the labels of the time-courses (L and H) 2000 times and an alpha-level of 0.05 was used to identify the significant clusters over time (Gerber, 2022). The same analyses were also run as supplementary analyses on the 1-second-long epoch to expand the investigation to the post-IED signal.

On the clusters of time-points identified by the significance test, we calculated the number of harmonics that are necessary to reconstruct 80% of the average energy ($N_{80\%}$) as a measure of the compactness of the signal, which was shown to be maximal when brain activity is integrated (rather than segregated) (Rué-Queralt et al., 2021). For each patient, the gPSD was computed on the portion of the signal identified by the cluster-based permutation test and it was used to sort the harmonics in descending order. Then we calculated the l2-norm over the harmonic dimension, using $M = 1, \cdots, N$ harmonics. $N_{80\%}$ was defined as the total number of NH necessary to reconstruct 80% of the total energy (where the total energy is the l_2-norm calculated -over the timepoints of the cluster and over the epochs- using all NHs) and a Wilcoxcon signed-rank test was used to compare $N_{80\%}$ between the clusters.

2.6.2. Broadcasting analyses and permutation test

Supplementary analyses include testing the broadcasting direction (BD) of the graph-filtered signal against 1000 degree-preserving surrogate SCs, computed with the Brain Connectivity Toolbox function *null_model_und_sign* (Rubinov and Sporns, 2010) as previously proposed (Rué-Queralt et al., 2021).The BD reflects the prevalent type of broadcasting dynamics and is defined as the difference between $E_L(t)$ and $E_H(t)$. When BD > 1, LF harmonics are more strongly represented and global communication is the prevalent broadcasting profile. When BD < 1, HF harmonics are more strongly represented and functional specialization is the prevalent broadcasting profile (Avena-Koenigsberger et al., 2018). At each time-point, the empirical BD was compared with the null distribution obtained by projecting the ROI time-courses on the degree-preserving surrogate structural connectomes. The goal was to investigate whether (1) the directionality of the BD was consistent across patients; (2) the harmonics of the empirical structural connectome performed better than those obtained from the surrogate.

2.6.3. Local changes: Structural decoupling index

After investigating how the content of LF and HF harmonics changed *over time at the whole-brain level*, we studied the nature of this content locally, i.e. for each ROI (averaged over time). The SDI was indeed calculated as the ratio between the norms of $x_{D,e}(t)$ and $x_{C,e}(t)$ over time, averaged over epochs (Preti and Van De Ville, 2019), for each brain region over the whole epoch (400 ms). For the analyses we used the binary logarithmic value of this index, so that a value of 0 corresponds to a perfect balance between SF coupling and decoupling, while positive/negative values represent decoupled/coupled regions and quantify the number of times "decoupling vs coupling"/"coupling vs. decoupling" is present in one region (e.g., 1 = double decoupling with respect to coupling).

Since the SDI is a ROI-specific feature, we decided to group patients according to the lateralization of the epilepsy. For each of the groups (RTLE and LTLE, N = 9 and N = 8 respectively), we selected the ROIs that were significantly coupled/decoupled over the whole 400 ms epoch with respect to surrogate graph signals, as previously described (Pirondini et al., 2016; Preti and Van De Ville, 2019). Briefly, we compared the empirical SDI of each ROI with the SDI of 19 surrogate time-courses, generated for each patient and epoch. The surrogate data $x_{rand,e}(t)$ were reconstructed with the iGFT, but we randomized the signs of the graph spectral coefficients by multiplying the harmonics of the structural connectome by *PHI*, a diagonal matrix with random + 1/-1 values:

$$x_{rand,e}(t) = U * \widehat{x}_{rand,e}(t) = U * PHI * \widehat{x}_e(t) = U * PHI * U^T * x_e(t)$$

In this way, interactions between NHs are randomized but the non-stationarity of the EEG data and correlations between time-points are maintained. Once surrogate time-courses are generated for each epoch and subject, the SDI is calculated as described above over the whole 400 ms epoch.

To define the brain regions that were significantly more coupled or decoupled than in the surrogate time-courses, we determined, for each ROI, the number of individuals that had a SDI bigger than the most decoupled surrogate or smaller than the most coupled one, with a probability of occurrence of $p = 1/(1 + 19) = 0.05$. Then, we used the binomial distribution $P(n)$ of having n detections to threshold the average SDI across individuals, for both groups (RTLE and LTLE). For a significance of 0.05, we retained only the ROI that were more coupled/decoupled than surrogates in at least 3 patients, for each group. Considering the small sample size of this study, we also use a more conservative threshold by retaining only the ROI more coupled/decoupled in 75% of patients in each group.

2.6.4. Local SDI changes across time (between clusters)

To test our hypothesis that the level of coupling/decoupling increases during the IED versus 'immediately before it', we calculated the SDIs of each ROI over the time windows detected by the cluster-based permutation test and compared them with a one-side Wilcoxon test. Given the small sample size, we reduced the number of comparisons by testing the SDI only for those regions that were significantly coupled/decoupled in at least 75% of participants for each group, which corresponded to 6 (out of 8) for the LTLE group and 7 (out of 9) for the RTLE group. We applied a Bonferroni correction according to the number of ROIs tested in each group.

In summary, we first identify significant time windows with cluster-based permutation test (Section 2.6.1). Then we look at the spatial changes by comparing the SDI with surrogate time series (used to retain only the most significant brain regions, Section 2.6.3). And then we merge this information, and we look at how those most significant ROI change between significant temporal clusters (Section 2.6.4).

3. Results

3.1. Segregation and integration along the IED

The cluster-based permutation test identified two clusters, cluster 1 (C1, ($p < .001$)) and cluster 2 (C2, $p < .05$), during which the energy contained in the HF harmonics was different from that contained in the LF harmonics (see Fig. 3). The first significant cluster C1, in the time window preceding the IED, shows that the energy of the whole-brain signal is concentrated in the upper end of the spectrum, i.e. HF harmonics explain most of the functional signal. C1 highlights a time window characterized by high-frequency harmonics corresponding to increased segregation patterns. Conversely, the second cluster C2 shows a significant predominance of LF harmonics from the IED half-rise until after the IED peak. This time window, represented mostly by smooth spatial maps, points at a predominance of integrative patterns. In the 1-second epoch, the supplementary analyses confirm these results. In addition, they show that the distribution of signal energy that characterizes the post-IED time window returns to pre-spike level, with predominance of HF harmonics (Fig. S1).
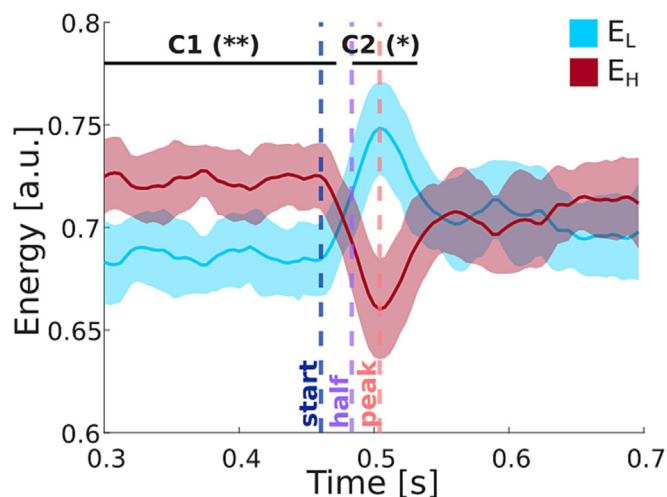

Fig. 3. The normalized energy of the ROI time-courses contained in the lower ($E_L(t)$, in blue) and higher ($E_H(t)$, in red) end of the spectrum. The black lines indicate a significant cluster of time points where the content of the low frequency harmonics and the high frequency ones is significantly different across patients. Asterisks (** and *) indicate significance, respectively $p < .001$ and $p < .05$. The vertical dashed lines indicate the start, half and peak of the average IED, across epochs and patients.

Moreover, the comparison of the number of harmonics necessary to reconstruct 80% of the average energy ($N_{80\%}$) during C1 and C2 confirmed that the functional signal is more compact during C2 or, in other words, represented by fewer spatial patterns (Fig. S2, $p < .001$). The higher compactness of the signal in C2 further points at integration as the prevalent mechanisms occurring during C2.

Indeed, the comparison of the broadcasting direction with the surrogate functional signals showed that all patients have a predominance of the low frequency harmonics during the spike, while the pre-spike time window is generally characterized by a prevalence of high frequency harmonics. This comparison was only significant in some patients and time-points although a trend was observed in all subjects (see Fig. S3).

3.2. Epileptic activity in ipsilateral mesial regions become more coupled during the spike

Our comparison of the empirical and surrogate structural-decoupling index shows that epileptic activity in mesial temporal regions over the 400 ms epoch is significantly coupled to the underlying structure even when using a more conservative threshold (see Fig. 4). Moreover, their level of coupling is higher in the ipsilateral hemisphere, as more intense shades of blue show in Fig. 4. When applying the more conservative threshold (75% of patients for each group), no region stands out as significantly decoupled (compared to surrogates), while the ipsilateral mesial regions result significantly coupled to the structure. Specifically, when using the most conservative threshold, 10 ROIs resulted significantly coupled to the structure in RTLE (among which featured the ipsilateral hippocampus, entorhinal cortex, amygdala, temporal pole and parahippocampal gyrus) and 7 in LTLE (including ipsilateral hippocampus, entorhinal cortex and insula), as shown in the second row of Fig. 4.

When we looked at local changes in time, we compared the SDI of the ROI that are more coupled than the best performing surrogate in at least 75% of each group (see blue regions in Fig. 5). The results revealed that some ipsilateral mesial ROI increased their level of coupling in C2 with respect to C1 (see Fig. 5, where a *decrease* of SDI correspond to an *increase* in coupling to the structure). Specifically, in the LTLE group, the left hippocampus was significantly more coupled -across patients- during C2 rather than C1 ($p < .05$, Bonferroni corrected for 7 comparisons, see Fig. 5b). Similarly, in the RTLE group, the right hippocampus, entorhinal cortex as well as left rostral anterior cingulate (RAC) increased their level of coupling during C2, with respect to C1 ($p < .05$, Bonferroni corrected for 10 comparisons, see Fig. 5d).

4. Discussion

Using GSP, we studied interictal activity in TLE in relation to its link to the underlying brain architecture, decomposed into patterns of structural harmonics. First, we found that the pre-spike window is characterized by the predominance of high-frequency harmonics while in the IED window, low-frequency harmonics contribute more strongly. Second, we found that activity of ipsilateral mesial regions is significantly coupled to the structure in most patients, while no significant decoupling was found with more conservative thresholds. Finally, we found that the level of coupling in the ipsilateral hippocampus (for both groups) and entorhinal cortex (for RTLE) increases from the pre-spike timepoints to the peak of the spike.

GSP and connectome analyses have recently been used to investigate resting state and cognitive processes tracked by fMRI and
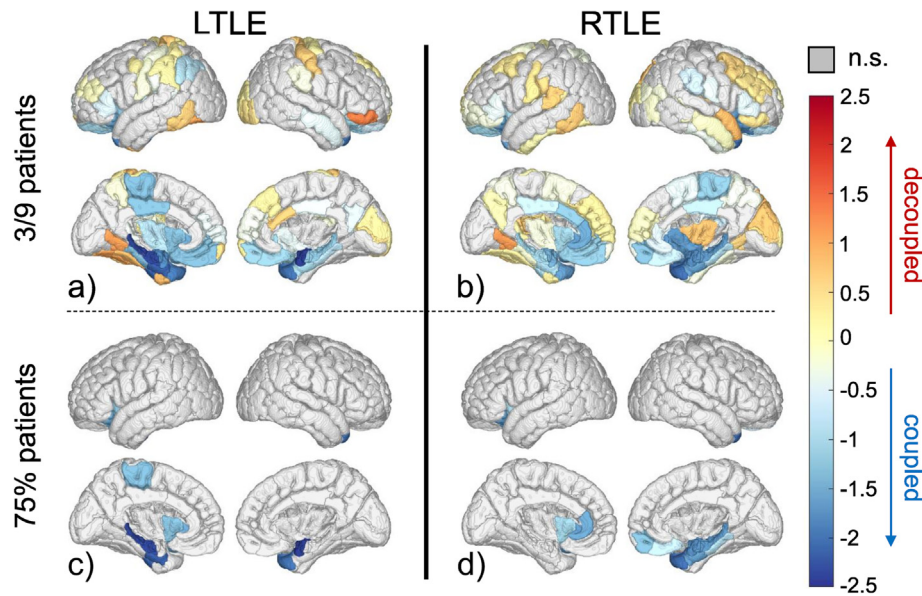
Fig. 4. Significant structural-decoupling index (SDI) values, calculated on the whole IED epoch in left TLE (LTLE, left column, (a) and (c)) and right TLE (RTLE, right column, (b) and (d)). The SDI is reported in binary logarithmic scale so a value of -2 indicates that the level of coupling of the specific ROI is 4 times as big as its level of decoupling. Regions reported in gray are not significantly coupled/decoupled (vs surrogate data). In the first row, (a) and (b), we retain the ROIs that were significantly more coupled/ decoupled than in the surrogate functional signals in at least 3 subjects. In the second row, we keep ROI significantly coupled/decoupled in at least 75% of the subjects, which corresponds to 6 out of 8 subjects for the LTLE (c) and 7 out of 9 subjects for the RTLE group (d).

EEG (Glomb et al., 2021, 2020; Griffa et al., 2022; Preti and Van De Ville, 2019; Rué-Queralt et al., 2021). However, to the authors' knowledge, this is the first application to interictal discharges in epilepsy. On top of strengthening the recent evidence on increased SF coupling during interictal and ictal activity based on intracranial recordings (Shah et al., 2019; Sinha et al., 2022), our non-invasive, whole brain, dynamic study suggests that this level of coupling shows transient changes *during* IEDs.

Low frequency harmonics have been interpreted as integrative patterns of neural activity in which brain regions communicate with each other via strong long-range couplings, assuming that the functional signal actually propagates through the structural connections (Avena-Koenigsberger et al., 2018). On the other hand, high frequency harmonics represent short-range coupling and, in this sense reflect more localized and segregative patterns. Here, the fact that most of the energy was found to be concentrated toward the higher harmonics before the IED (C1) and then toward the lower ones during the IED (C2), suggests a radical change in functional network organization occurring during IED. In other words, the brain activity seems fragmented and sparsely localized before the discharge, and therefore relies on coarse spatial patterns, or segregative mechanisms. When the spike occurs, a smoother and more long-range network, more linked to the underlying structure, seems to be recruited – possibly to play out the propagation of the epileptic activity to the rest of the epileptogenic network- in what could be seen as an integrative process. Supplementary analyses show that, although the empirical NHs do not outperform surrogate ones for every time point and patient, the transition between HF and LF harmonics is consistent across patients (see Fig. S3). Increased integration of brain activity during IEDs –as reflected by the global efficiency of the brain network- was indeed reported in TLE patients with worse post-operative outcome, suggesting that the extent of the efficiency of the information transfer across the brain reflected a more spread (smooth, long-range) epileptogenic network (Carboni et al., 2019). As further evidence in support of this interpretation, we showed that compactness of the ROI time-courses in C2 is higher than in C1, i.e. fewer harmonics are sufficient to explain 80% of the energy of

the signal in C2 than in C1. When GSP was applied to visual evoked potentials, the compactness of the functional ROI signals was inversely correlated to the amount of energy concentrated in the higher end of the spectrum (Rué-Queralt et al., 2021).

To shed light on the spatial detail, we calculated, for each brain region, the ratio between the energy of its decoupled and coupled time courses and thresholded the ROIs by comparing their SDI with those of surrogate time series. The least conservative threshold retained a wide variety of both coupled and decoupled ROIs, with the latter showing no clear spatial pattern across the groups. When the more conservative threshold was used instead, only coupled ROIs were retained (Fig. 4, second row). Specifically, when retaining only the ROIs significantly coupled in at least 75% of the subjects it can be noticed that the sole brain regions retained are the mesial ones, mostly located in the ipsilateral hemisphere. Interestingly, these brain regions are characterized by very low SDI values, meaning that the LF harmonics (smooth spatial maps) express most of their time-course. Read in the context of our TLE cohort mostly diagnosed with hippocampal sclerosis (HS), the ipsilateral mesial regions coupled to the structure could reflect critical nodes with long-range coupling in the epileptogenic network. Further studies are warranted to assess whether this coupling is also present during background EEG activity between IEDs and how it deviates from controls subjects.

Studying the SDI changes in the two time-windows identified by the cluster-based permutation test, C1 (pre-IED) and C2 (IED peak), we found that the ipsilateral hippocampus (and also ipsilateral entorhinal cortex and contralateral rostral anterior cingulate for the RTLE group), which are strongly coupled during C1, become even more coupled during C2. This coupling enhancement during the IED is in line with previous EEG-fMRI studies. Similar connectivity patterns were found among fMRI-derived functional connectivity (FC) maps between runs with or without visible IED on scalp EEG, suggesting that the underlying network originating and supporting the spread of the IED is constantly embedded but more strongly recruited in occurrence of the IEDs (Luo et al., 2014). Similarly, FC maps were preserved with and without the contribution of the epileptic discharge, with a significant reduction in connec-
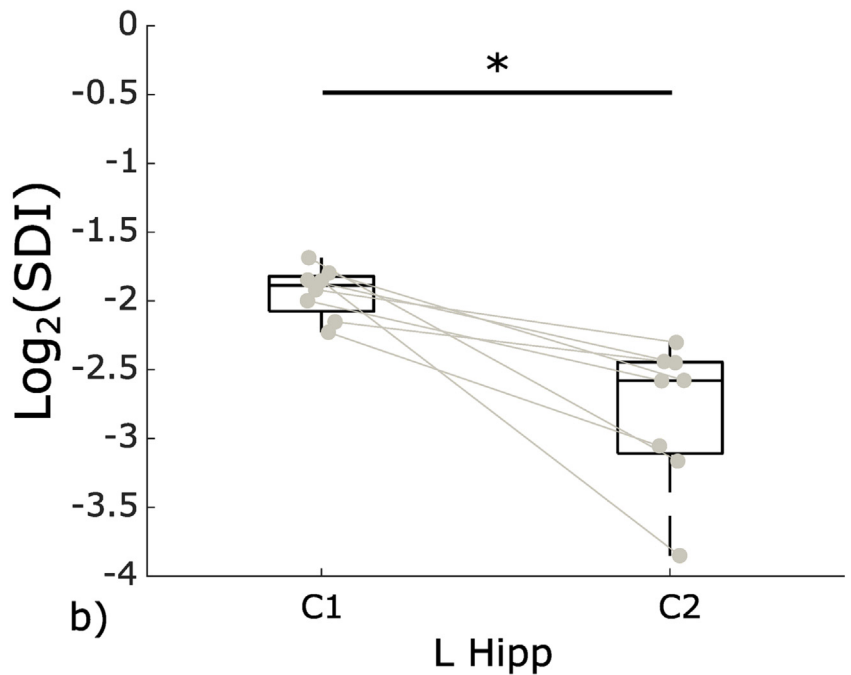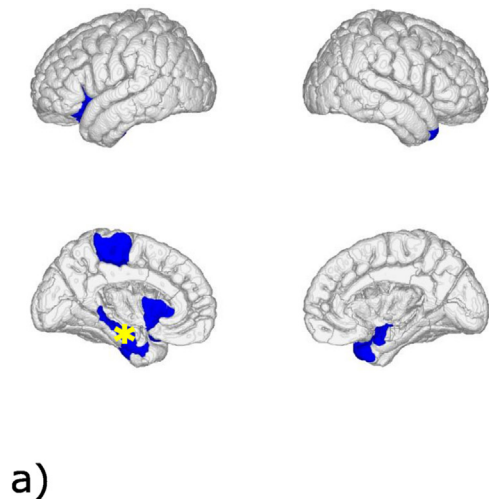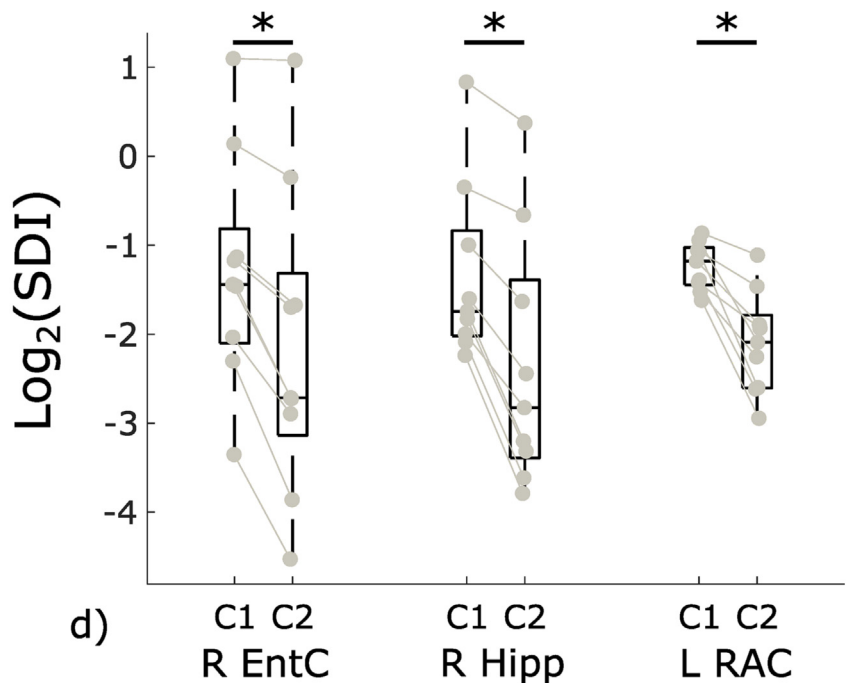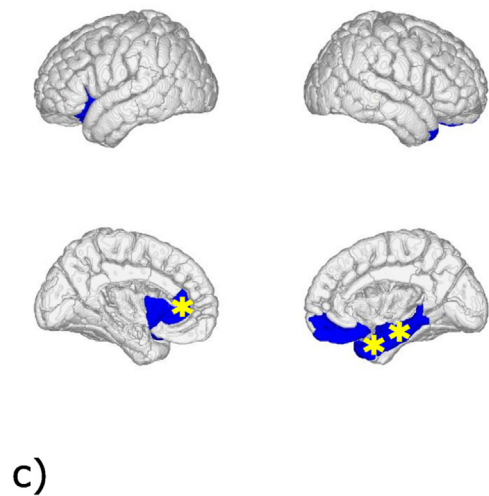
Fig. 5. Changes of the structural-decoupling index (SDI) values, in specific region of interest (ROI), between the two clusters in the left TLE (LTLE) and right TLE (RTLE) group (top and bottom line, respectively). Figures on the left show the ROI that were tested for the LTLE group (a) and the RTLE group (c), where ROI depicted in blue are those that were more coupled than surrogates in at least 75% of the patients. Yellow asterisks indicate the ROI for which the SDI changed significantly between C1 and C2. Figures on the right, (b) and (d), show the boxplots of the logarithmic value of the SDI for the ROI that significantly changed from C1 to C2: asterisks indicate statistical significance ($p < .05$). Hipp = hippocampus; EntC = entorhinal cortex; RAC = rostral anterior cingulate.

tivity values when the IED contribution was regressed out (Iannotti et al., 2016) and with a strengthening of some connections correlated to IED occurrence (Iannotti et al., 2020). In line with these findings, our results suggest that an increased recruitment of this network is observable during the IED.

Altogether, at the whole-brain level, our analyses are able to distinguish between segregative patterns – preceding the IED – and integrative patterns – during the IED – indicating a switch between very different network configurations at a global level. However, when looking at each ROI individually, we find that the

electrical activity of brain regions that are likely to be highly involved in the epileptogenic network (generation and propagation of the IED) –hippocampus and entorhinal cortex- is predominantly coupled to the structural connectome, rather than decoupled, and that this coupling significantly increases during the IED. This suggests that the mesial regions are likely to constantly belong to this network (and therefore be coupled even before the beginning of the spike), but the smooth (long range) spatial maps are recruited more during the spike. It remains unknown whether this is part of a large scale permissive mechanisms for the IED occurrence or the consequence of the IED allowing the transfer of the information to other brain regions via long range coupling. Future studies could extend these analyses to longer 'pre-IED' segments, or even to segments without IEDs, to investigate if the background coupling level of ipsilateral mesial temporal regions is indeed constant and whether it differs from that of healthy controls. If these differences in SF coupling persist even in the absence of scalp-visible IEDs, the coupling between brain architecture and EEG could constitute a potential biomarker for epilepsy. Moreover, future studies should expand this investigation to a more heterogeneous population, including extra-temporal epilepsies and more patients who did not achieve seizure-freedom after the surgery to investigate the clinical relevance of SF coupling in epilepsy.

Limitations

The small sample size of the study represents one of the main limitations. However, the highly conservative approach used to threshold brain region SDI should ensure robustness. Indeed, choosing to threshold the ROIs to those that are significantly more coupled/decoupled than the surrogates in 75% of subjects corresponds to a p value of $1e^{-44}$ and $1e^{-36}$, for RTLE (7/9 patients) and LTLE (6/8 patients) respectively.

Another potential limitation relates to the reconstruction of cortical electrical activity based on scalp EEG. ROI-based time-courses are smooth and therefore LF harmonics represent most of the energy of the signal. We addressed this issue by dichotomizing the connectome spectrum in two halves of equal energy rather than simply dividing the set of harmonics in two. Moreover, the connectome spectrum was shown to be the most robust representation to this bias by comparing compactness performance in empirical and white-noise data across ROI-based representation, connectome spectrum representation and Euclidean distance harmonic representation (Rué-Queralt et al., 2021). The inclusion of subcortical regions would be easy in the structural connectome but poses important challenges and uncertainties for the reconstruction of source activity. Including dummy subcortical structures (functional signals set to zero) would practically change the structural connectivity graph (and therefore the harmonics themselves) but their contribution (to each network harmonic) would be zeroed during the GFT. In this first clinical application of EEG-based GFP we preferred to stick to the previously proposed methodology (Glomb et al., 2020; Rué-Queralt et al., 2022a, 2022b).

We used a consensus structural connectome obtained from healthy subjects. Arguably, this could be seen as another limitation of the study but actually carries some advantages. On the one hand, it is known that structural differences exist in patients with TLE, such as decreased fractional anisotropy and increased mean diffusivity (Slinger et al., 2016) or that pathologic SCs are less integrated than healthy ones (Slinger et al., 2021). The use of NHs extracted from patient-specific SC could therefore be seen as definite methodological improvement. On the other however, high-quality diffusion MRI data is difficult to obtain in clinical settings and its reconstruction at the individual level would lead to false

positive connections and a variability of bases to project the EEG traces onto. Importantly the eigenvectors of the SC (network harmonics) are used in large groups of frequency values (LF vs HF) and no single harmonic is used to infer on the network underlying the IED. Therefore, we consider that using a slightly different SC would provide only slightly different harmonics and would not yield different results as to whether the energy of the signal is allocated in LF or HF harmonics. For future studies, a consensus SC obtained from TLE patients is probably the most robust option to consider.

Author contributions

IR: Conceptualization; Data curation; Methodology; Formal analysis; Writing – original draft; Writing – review & editing. **JRQ**: Data curation; Methodology; Writing – review & editing. **KG**: Methodology; Writing – review & editing. **GMP**: Methodology; Writing – review & editing. **TS**: Software; Writing – review & editing. **NR**: Software; Writing – review & editing. **LS**: Resources. **MS**: Resources; Writing – review & editing. **DVD**: Funding acquisition; Writing – review & editing. **PH**: Conceptualization; Funding acquisition; Writing – review & editing. **SV**: Conceptualization; Supervision; Funding acquisition; Writing – review & editing.

Declaration of Competing Interest

MS has shares in Epilog and received speaker's fees from UCB. **SV** has shares in Epilog.

Acknowledgements

Data and materials availability

The source-reconstructed data and the consensus structural connectome are available on Zenodo at https://doi.org/10.5281/zenodo.8005116. Raw data can be made fully available upon reasonable request to SV within the limits of ethical regulations of Switzerland. As such the project of the requesting party will need to undergo formal ethical approval at the local site with regulations compatible with those at our centre.

The code used can be found at https://github.com/IsottaR/SFcoupling_IED_GSP.

Appendix A. Supplementary material

Supplementary material to this article can be found online at https://doi.org/10.1016/j.clinph.2023.05.012.

References

Atasoy S, Donnelly I, Pearson J. Human brain networks function in connectome-specific harmonic waves. Nat Commun 2016;7. https://doi.org/10.1038/ncomms10340.

Avena-Koenigsberger A, Misic B, Sporns O. Communication dynamics in complex brain networks. Nat Rev Neurosci 2018;19:17–33. https://doi.org/10.1038/nrn.2017.149.

Bartolomei F, Lagarde S, Wendling F, McGonigal A, Jirsa V, Guye M, et al. Defining epileptogenic networks: Contribution of SEEG and signal analysis. Epilepsia 2017;58:1131–47. https://doi.org/10.1111/epi.13791.

Cammoun L, Gigandet X, Meskaldji D, Thiran JP, Sporns O, Do KQ, et al. Mapping the human connectome at multiple scales with diffusion spectrum MRI. J Neurosci Methods 2012;203:386–97. https://doi.org/10.1016/j.jneumeth.2011.09.031.

Carboni M, Rubega M, Iannotti GR, De Stefano P, Toscano G, Tourbier S, et al. The network integration of epileptic activity in relation to surgical outcome. Clin Neurophysiol 2019;130:2193–202. https://doi.org/10.1016/j.clinph.2019.09.006.

Carboni M, De Stefano P, Vorderwülbecke BJ, Tourbier S, Mullier E, Rubega M, et al. Abnormal directed connectivity of resting state networks in focal epilepsy. NeuroImage Clin 2020;27. https://doi.org/10.1016/j.nicl.2020.102336 102336.

Chiang S, Stern JM, Engel J, Haneef Z. Structural-functional coupling changes in temporal lobe epilepsy. Brain Res 2015;1616:45–57. https://doi.org/10.1016/j.brainres.2015.04.052.

Gerber EM. permutest (https://www.mathworks.com/matlabcentral/fileexchange/71737-permutest), MATLAB Central File Exchange; Retrieved May 3, 2022.

Glomb K, Kringelbach ML, Deco G, Hagmann P, Pearson J, Atasoy S. Functional harmonics reveal multi-dimensional basis functions underlying cortical organization. Cell Rep 2021;36. https://doi.org/10.1016/j.celrep.2021.109554 109554.

Glomb K, Rué Queralt J, Pascucci D, Defferrard M, Tourbier S, Carboni M, et al. Connectome spectral analysis to track EEG task dynamics on a subsecond scale. Neuroimage 2020;221. https://doi.org/10.1016/j.neuroimage.2020.117137.

Gramfort A, Papadopoulo T, Olivi E, Clerc M. Forward field computation with OpenMEEG. Comput Intell Neurosci 2011;2011. https://doi.org/10.1155/2011/923703.

Griffa A, Alemán-Gómez Y, Hagmann P. Structural and functional connectome from 70 young healthy adults. Zenodo 2019. https://doi.org/10.5281/zenodo.2872624.

Griffa A, Amico E, Liégeois R, Van De Ville D, Preti MG. Brain structure-function coupling provides signatures for task decoding and individual fingerprinting. Neuroimage 2022;250. https://doi.org/10.1016/j.neuroimage.2022.118970 118970.

Hagmann P, Cammoun L, Gigandet X, Meuli R, Honey CJ, Van Wedeen J, et al. Mapping the structural core of human cerebral cortex. PLoS Biol 2008;6:1479–93. https://doi.org/10.1371/journal.pbio.0060159.

Iannotti GR, Grouiller F, Centeno M, Carmichael DW, Abela E, Wiest R, et al. Epileptic networks are strongly connected with and without the effects of interictal discharges. Epilepsia 2016;57:1086–96. https://doi.org/10.1111/epi.13400.

Iannotti GR, Preti MG, Grouiller F, Carboni M, De Stefano P, Pittau F, et al. Modulation of epileptic networks by transient interictal epileptic activity: A dynamic approach to simultaneous EEG-fMRI. NeuroImage Clin 2020;28. https://doi.org/10.1016/j.nicl.2020.102467 102467.

Lagarde S, Roehri N, Lambert I, Trebuchon A, McGonigal A, Carron R, et al. Interictal stereotactic-EEG functional connectivity in refractory focal epilepsies. Brain 2018;141:2966–80. https://doi.org/10.1093/brain/awy214.

Laufs H. Functional imaging of seizures and epilepsy: Evolution from zones to networks. Curr Opin Neurol 2012;25:194–200. https://doi.org/10.1097/WCO.0b013e3283515db9.

Luo C, An D, Yao D, Gotman J. Patient-specific connectivity pattern of epileptic network in frontal lobe epilepsy. NeuroImage Clin 2014;4:668–75. https://doi.org/10.1016/j.nicl.2014.04.006.

Maris E, Oostenveld R. Nonparametric statistical testing of EEG- and MEG-data. J Neurosci Methods 2007;164:177–90. https://doi.org/10.1016/j.jneumeth.2007.03.024.

Oostenveld R, Fries P, Maris E, FieldTrip SJM. Open source software for advanced analysis of MEG, EEG, and invasive electrophysiological data. Comput Intell Neurosci 2011;2011. https://doi.org/10.1155/2011/156869.

Ortega A, Frossard P, Kovacevic J, Moura JMF, Vandergheynst P. Graph signal processing: Overview, challenges, and applications. Proc IEEE 2018;106:808–28. https://doi.org/10.1109/JPROC.2018.2820126.

Perrin F, Pernier J, Bertrand O. Spherical splines for scalp potential and current density mapping. Electroencephalogr Clin Neurophysiol 1989;72:184–7.

Pirondini E, Vybornova A, Coscia M, Van De Ville D. A spectral method for generating surrogate graph signals. IEEE Signal Process Lett 2016;23:1275–8. https://doi.org/10.1109/LSP.2016.2594072.

Preti MG, Van De Ville D. Decoupling of brain function from structure reveals regional behavioral specialization in humans. Nat Commun 2019;10:1–7. https://doi.org/10.1038/s41467-019-12765-7.

Rubega M, Carboni M, Seeber M, Pascucci D, Tourbier S, Toscano G, et al. Estimating EEG source dipole orientation based on singular-value decomposition for connectivity analysis. Brain Topogr 2019;32:704–19. https://doi.org/10.1007/s10548-018-0691-2.

Rubinov M, Sporns O. Complex network measures of brain connectivity: Uses and interpretations. Neuroimage 2010;52:1059–69. https://doi.org/10.1016/j.neuroimage.2009.10.003.

Rué-Queralt J, Fluhr H, Tourbier S, Aleman-gómez Y, Pascucci D. Connectome spectrum electromagnetic tomography: a method to reconstruct electrical brain sources at high-spatial resolution. BioRxiv 2022. https://doi.org/10.1101/2022.07.26.501544 2022.07.26.501544.

Rué-Queralt J, Glomb K, Pascucci D, Tourbier S, Carboni M, Vulliémoz S, et al. The connectome spectrum as a canonical basis for a sparse representation of fast brain activity. Neuroimage 2021;244. https://doi.org/10.1016/j.neuroimage.2021.118611 118611.

Rué-Queralt J, Mancini V, Rochas V, Latrèche C, Uhlhaas PJ, Michel CM, et al. Neural integration and segregation revealed by a joint time-vertex connectome spectral analysis. BioRxiv 2022. https://doi.org/10.1101/2022.07.26.501543 2022.07.26.501543.

Shah P, Ashourvan A, Mikhail F, Pines A, Kini L, Oechsel K, et al. Characterizing the role of the structural connectome in seizure dynamics. Brain 2019;142:1955–72. https://doi.org/10.1093/brain/awz125.

Shuman DI, Narang SK, Frossard P, Ortega A, Vandergheynst P. The emerging field of signal processing on graphs. IEEE Signal Process Mag 2013;30:83–98.

Sinha N, Duncan JS, Diehl B, Chowdhury FA, de Tisi J, Miserocchi A, et al. Intracranial EEG structure-function coupling predicts surgical outcomes in focal epilepsy. ArXiv 2022. arXiv:2204.08086.

Slinger G, Otte WM, Braun KPJ, van Diessen E. An updated systematic review and meta-analysis of brain network organization in focal epilepsy: Looking back and forth. Neurosci Biobehav Rev 2021. https://doi.org/10.1016/j.neubiorev.2021.11.028.

Slinger G, Sinke MRT, Braun KPJ, Otte WM. White matter abnormalities at a regional and voxel level in focal and generalized epilepsy: A systematic review and meta-analysis. NeuroImage Clin 2016;12:902–9. https://doi.org/10.1016/j.nicl.2016.10.025.

Sorrentino P, Seguin C, Rucco R, Liparoti M, Lopez ET, Bonavita S, et al. The structural connectome constrains fast brain dynamics. Elife 2021;10:1–11. https://doi.org/10.7554/eLife.67400.

Pascual-Marqui RD. Discrete, 3D distributed, linear imaging methods of electric neuronal activity. Part 1: exact, zero error localization. ArXiv 2007: arXiv:0710.3341. https://arxiv.org/abs/0710.3341

Tourbier S, Aleman-Gomez Y, Griffa A, Bach Cuadra M, Hagmann P. connectomicslab/connectomemapper3: Connectome Mapper v3.0.0-beta-20200206. 2020. https://doi.org/10.5281/ZENODO.3653749.

Tourbier S, Rue-Queralt J, Glomb K, Aleman-gomez Y, Mullier E, Griffa A, et al. Connectome Mapper 3: A flexible and open-source pipeline software for multiscale multimodal human connectome mapping. J Open Source Softw 2022;7:4248. https://doi.org/10.21105/joss.04248.

Trimmel K, Vos SB, Caciagli L, Xiao F, van Graan LA, Winston GP, et al. Decoupling of functional and structural language networks in temporal lobe epilepsy. Epilepsia 2021;62:2941–54. https://doi.org/10.1111/epi.17098.

Vorderwülbecke BJ, Carboni M, Tourbier S, Brunet D, Seeber M, Spinelli L, et al. High-density electric source imaging of interictal epileptic discharges: How many electrodes and which time point? Clin Neurophysiol 2020;131:2795–803. https://doi.org/10.1016/j.clinph.2020.09.018.

Wang R, Lin P, Liu M, Wu Y, Zhou T, Zhou C. Hierarchical connectome modes and critical state jointly maximize human brain functional diversity. Phys Rev Lett 2019;123. https://doi.org/10.1103/PhysRevLett.123.038301 38301.

Wedeen VJ, Wang RP, Schmahmann JD, Benner T, Tseng WYI, Dai G, et al. Diffusion spectrum magnetic resonance imaging (DSI) tractography of crossing fibers. Neuroimage 2008;41:1267–77. https://doi.org/10.1016/j.neuroimage.2008.03.036.

Wirsich J, Perry A, Ridley B, Proix T, Golos M, Bénar C, et al. Whole-brain analytic measures of network communication reveal increased structure-function correlation in right temporal lobe epilepsy. NeuroImage Clin 2016;11:707–18. https://doi.org/10.1016/j.nicl.2016.05.010.